

Scanning micro X-ray diffraction unveils the distribution of oxygen chains nano-puddles in $\text{YBa}_2\text{Cu}_3\text{O}_{6.33}$

Gaetano Campi¹, Alessandro Ricci², Nicola Poccia³, Luisa Barba⁴, G. Arrighetti⁴, Manfred Burghammer⁵, A.-S. Caporale⁶, Antonio Bianconi^{6,7}

¹*Institute of Crystallography, CNR, via Salaria Km 29.300, Monterotondo Roma, 00015, Italy*

²*Deutsches Elektronen-Synchrotron DESY, Notkestraße 85, D-22607 Hamburg, Germany.*

³*MESA+ Institute for Nanotechnology, University of Twente, P. O. Box 217, 7500AE Enschede, Netherlands.*

⁴*Elettra Sincrotrone Trieste. Strada Statale 14 - km 163, 5, AREA Science Park, 34149 Basovizza, Trieste, Italy*

⁵*European Synchrotron Radiation Facility, B. P. 220, F-38043 Grenoble Cedex, France.*

⁶*RICMASS Rome International Center for Materials Science Superstripes, via dei Sabelli 119A, 00185 Roma, Italy*

⁷*Physics Dept., Sapienza University of Rome, 00185 Roma, Italy*

Oxygen chain fragments are known to appear at the insulator-to-superconductor transition (SIT) in $\text{YBa}_2\text{Cu}_3\text{O}_{6+y}$. However the self organization and the size distribution of oxygen chain fragments is not known. Here we contribute to fill this gap, using scanning micro-X-ray diffraction a novel non invasive imaging method based on advances in focusing synchrotron radiation beam. This novel approach allows us to probe both real-space and k-space of high-quality $\text{YBa}_2\text{Cu}_3\text{O}_{6.33}$ single crystals with $T_c=7\text{K}$. We report compelling evidence for a nematic phase of nanoscale striped puddles with Ortho-II structure made of chain fragments in the basal $\text{Cu}(1)$ plane with local oxygen concentration $y \geq 0.5$. The size of the Ortho-II puddles span a range between 2 and 9 nanometers. The real space imaging with micron resolution of the granular network of Ortho-II puddles shows that superconductivity at low hole doping in this system occurs in an inhomogeneous network of nanoscale oxygen ordered patches interspersed with oxygen depleted regions. The manipulation by thermal treatments of the Ortho-II puddles has been investigated focusing on their formation and evolution at the order-to-disorder phase transition at $T=350\text{K}$.

Introduction. High temperature superconductivity (HTS) appears in composite materials made of stacks of active superconducting layers intercalated by spacer layers [1]. In $\text{YBa}_2\text{Cu}_3\text{O}_{6+y}$ (YBCO) [2] the active layers are made of an infinite layer cuprate, $\text{Y}[\text{Cu}(2)\text{O}_2]_2$, intercalated with the spacer oxide block made of a defective rocksalt oxide, $[\text{BaO}]_2\text{Cu}(1)\text{O}_{i_y}$. In the defective spacer oxide block the oxygen defect ions O_{i_y} partially fill the empty basal plane sites. In-homogeneity is a generic feature of HTS because of the electronic phase separation near the charge transfer Mott phase: where metallic stripes [3], hosting the doped holes with $\text{O}(2p^5)\text{Cu}(3d^9)$ configuration [4], coexist with antiferromagnetic domains. Moreover also the lattice diverges from the average structure [5] because of i) unscreened defects in the spacer layers; ii) corrugated CuO_2 short range nano-domains driven by polaronic local lattice distortions [6] and the lattice misfit strain between active and spacer blocks [7,8]. While in the past years lattice inhomogeneity was not considered an essential parameter in the search of the mechanism of HTS, recently the interest on the role of defects for controlling the critical temperature is growing [9]. While disorder usually suppresses the superconducting critical temperature in conventional superconductors an optimum lattice inhomogeneity has been found to enhance the critical temperature in HTS [10,11]. The tendency toward electronic phase separation in strongly correlated multiband systems with polaronic and Fermi particles near a Mott transition is now well accepted [12-15]. Recently several theories have been proposed based on the presence in HTS of networks of nanoscale superconducting grains [16-21]. The nanoscale phase separation related to the self-organization of defects is not a unique feature of cuprates

like super-oxygenated $\text{La}_2\text{CuO}_{4+y}$ [22] $\text{La}_{2-x}\text{Sr}_x\text{CuO}_4$ [6,23,24] and $\text{Bi}_2\text{Sr}_2\text{CaCu}_2\text{O}_{8+y}$ [25], but it has been found also in $\text{Al}_{1-x}\text{Mg}_x\text{B}_2$ [26], doped iron-chalcogenides [27-29], and other functional materials like manganites [30]. Thermal treatments to control defect organization [31-34] on photo-induced effects [35], muon-spin resonance (μSR) [36] showed that lattice complexity controls T_c in YBCO. However direct information concerning lattice inhomogeneity in YBCO [37] is missing because of lack of suitable experimental methods.

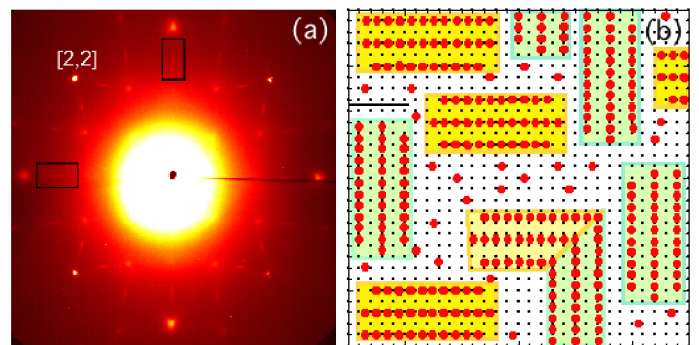


Figure 1. (Colored online) Panel (a): the diffraction pattern in the (h,k) plane of $\text{YBa}_2\text{Cu}_3\text{O}_{6.33}$ ($T_c=7\text{K}$). The diffuse streaks $q_{\text{ortho-II}}$ at $(h+0.5,0)$ are superstructure satellites due to nanoscale puddles with Ortho-II structure made by O_i ordering after annealing at 300K. The equal intensity of horizontal $[2.5,0]$ and vertical $[0,2.5]$ streaks highlighted with the black rectangles, indicate a nematic phase made of the Ortho-II puddles. Panel (b): Pictorial view of the horizontal and vertical oxygen rich ($y=0.5$) Ortho-II puddles intercalated by disordered oxygen poor ($y<0.33$) domains. The black bar indicates 2 nm length scale.

In this work we have used the novel scanning micro X-ray diffraction (μ XRD) [11,22] to unveil the lattice complexity in YBCO. We focus on the size distribution and imaging the spatial distribution of oxygen O_i chains fragments in the basal plane near the insulator-to-superconductor transition (SIT) and we study the effect of thermal treatments [38].

The Ortho-II satellite superstructure streaks in the XRD pattern of YBCO for $0.33 < y < 0.62$ [39-41] are analyzed to get the size of nano-scale Ortho-II puddles and their spatial distribution.

Materials and Methods. The single crystals of $YBa_2Cu_3O_{6.33}$ were grown using barium zirconate crucibles by the self-flux technique using chemicals of 99.999% purity for CuO and Y_2O_3 , and 99.997% for $BaCO_3$ [43,44]. The purity of the crystals was found to be better than 99.99 atomic % by analysis using inductively-coupled plasma mass spectroscopy. The oxygen content of the crystal was set to 6.33 by annealing in flowing oxygen at $914^\circ C$ followed by quenching to room temperature under flowing nitrogen gas. The macroscopic oxygen content inhomogeneity was removed by annealing the crystal at $570^\circ C$ in a tiny sealed quartz capsule followed by quenching to ice-water bath. The crystal was then kept at room temperature to let the short range oxygen order to develop [45].

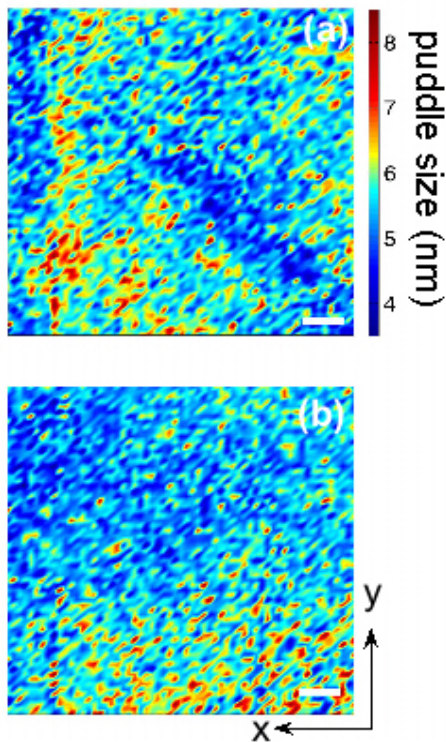


Figure 2. Scanning micro X-ray diffraction of a single crystal $YBa_2Cu_3O_{6.33}$: color map of the size of the Ortho-II oxygen chain puddles ranging from 3 (dark blue) to 9 (red) nanometers in the a-axis direction (panel a) and in the c-axis direction (panel b) measured by the FWHM of the reflection spots of the $1\mu m$ X-ray beam collected by the CCD detector probing the k-space. The width (color) of the Ortho-II puddles is plotted as a function of the illuminated spot position xy in the sample surface. The white bar indicates $20\mu m$ length scale on the sample surface.

The source of the 12.4 KeV X-rays for scanning μ XRD at the ID13 beamline of ESRF is an electron undulator. The crystal optics includes a tapered glass capillary. It produces a $1\mu m$ beam spot at the sample. A charge-coupled area detector (CCD) records the X-rays scattered by the sample.

Results. A typical X-ray synchrotron diffraction (XRD) pattern of the $YBa_2Cu_3O_{6.33}$ in transmission mode probing the bulk structure is depicted in Fig. 1a. The lattice parameters are: $a = 3.851(4)\text{ \AA}$, $b = 3.856(4)\text{ \AA}$, $c = 11.78(5)\text{ \AA}$. The Cu-O bond distance is 192.8 pm, showing a 2% compression relative with the Cu-O equilibrium distance of 197 pm [46]. Therefore this sample is near the optimum misfit strain [7,8] and the SIT transition. Visual inspection of the 2D diffraction pattern in Fig.1a shows immediately the needle shaped satellite reflections $q_{ortho-II}$ ($h \pm 0.5, k, l$) between the principal reflections associated with ordered oxygen chains fragments forming nanoscale Ortho-II puddles. The satellites of $q_{ortho-II}$ have a needle shape clearly pointing in both horizontal and vertical directions. The equal intensity of vertical and horizontal streaks indicate a nematic phase of horizontal and vertical puddles. A pictorial of the phase separation view derived from these data is shown in Fig. 1b. The oxygen rich O_i chain fragments form nanoscale ‘‘Ortho-II’’ puddles that coexist with oxygen poor domains with disordered O_i .

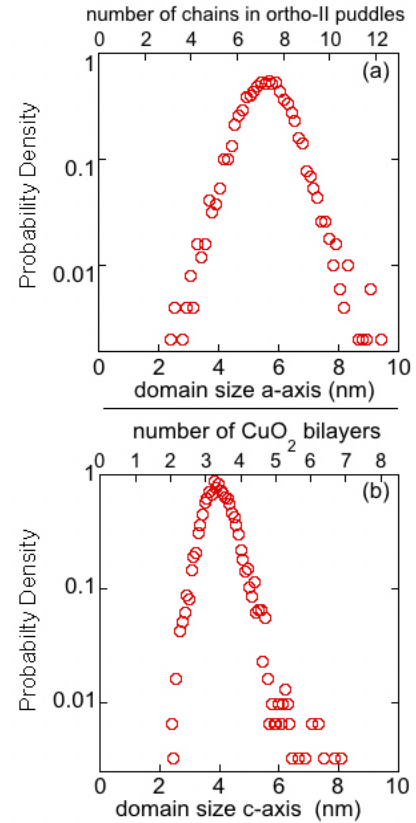


Figure 3. Statistical distribution of the size of the Ortho-II puddles from data shown in Fig. 2. Panels (a) and (b) show the probability distribution function of spots in the crystal where the Ortho-II puddles have the same size in the a-axis (c-axis in panel b) direction. The puddle size in nanometers, is determined from the FWHM of superstructure diffraction $q_{ortho-II}$ satellite reflections in the a^* (c^* in panel b) direction.

The domain size of the Ortho-II puddles in the illuminated micrometer area has been derived from the measured full width half maximum (FWHM) of the superlattice reflections via standard methods of diffraction [42]. The FWHM of diffraction profiles are measured at each point (x,y) of the sample reached by the x-y translator with micron resolution. Fig. 2 shows the spatial maps of the size of the nano-scale Ortho-II puddles. The statistical distribution of the size of the Ortho-II puddles is shown in Fig. 3.

The integrated intensity of the superstructure and the peak position of satellites in different spots of the crystal are quite homogenous, $q_{\text{ortho-II}}=0.5$ with a standard deviation of 0.001. This indicates that the nano-scale oxygen puddles have the Ortho-II periodicity and confirms the high quality of the crystal. On the contrary the FWHM of the diffraction profiles size of the diffracting nano-scale puddles is ranging between 3 and 9 nanometers from spot to spot.

Fig. 2 shows the real space mapping of the nanoscale Ortho-II puddles size plotting in the color scale their size derived from the inverse of the superstructure satellites FWHM in the k-space along the a^* (panel a), c^* (panel b) directions. A visual inspection of the mapping shows the heterogeneous granular structure. The probability distribution of the length of the chain fragments in Fig. 3a shows that the Ortho-II puddles are made of 2.5 to 12 oxygen chains indicating the different size of the puddles with a fat tail for the longer fragments.

The statistical distribution of the out-of-plane size of the Ortho-II puddles along the c crystallographic direction shows an average value of 4 nm and a standard deviation of 0.6 nm. We observe clear irregularities and deviations from normal behavior in the distribution tails. In order to quantify these deviation we have calculated the distribution skewness, sk , giving $sk_a=0.3$ and $sk_c=0.9$ for the Ortho-II domain size along the a and c directions, respectively. Their positive values indicate a larger weight of the right tails in both distributions, while the fact that sk_c is substantially larger than sk_a confirms accentuated disorder in the out of plane direction.

Having determined the spatial imaging and distributions of the Ortho-II puddles we move to the effects of thermal treatments using the XRD1 beamline of the ELETTRA synchrotron in Trieste (Italy). The diffraction pattern as a function of temperature were collected by means of a K-diffractometer with a motorized goniometric X-Y stage head and a Mar-Research 165 mm Charge Coupled Device (CCD) camera, 70 mm far from the sample. The 20 KeV X-ray beam was selected from the source by a double-crystal Si(111) monochromator. Figure 4a shows the three dimensional temperature evolution of the (0,2.5) Ortho-II satellite profile along h and k , respectively. The temperature of the crystals has been increased from 300K to 400 K, using a cryo-cooler (700 series Oxford Cryosystems). The heating cycle was carried out through a quite slow rate (0.2 K /minute). The raw data of cuts along the h and k directions in the k-space collected during the

heating ramp are shown in panels a) and b) of Fig. 4. The Ortho-II puddle shows the order to disorder phase transition at $T=350\pm 5$ K. The width of the diffraction profiles in k -direction in panel (c) probes the disorder in the chain direction (b-axis) i.e. the chain fragment length.

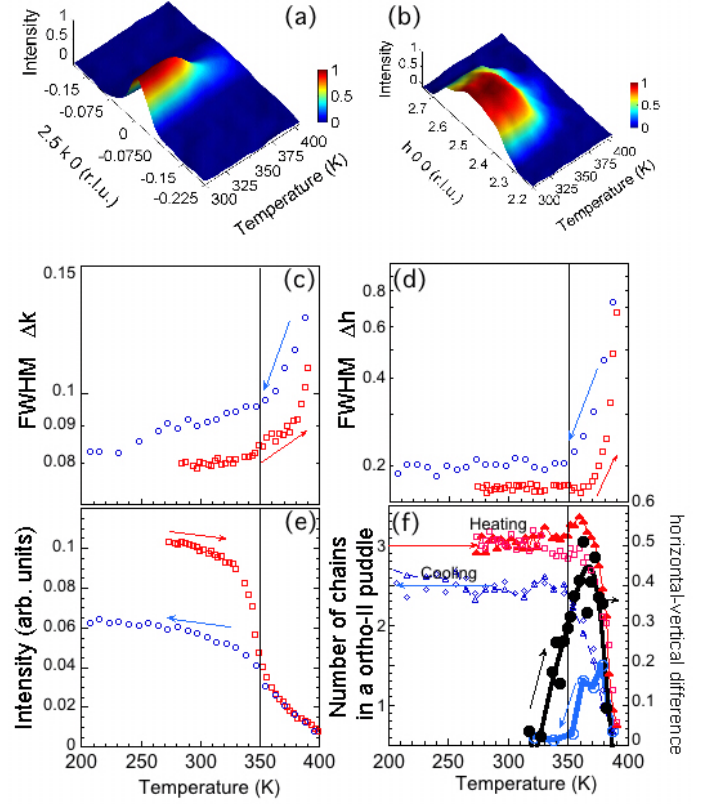


Figure 4. Temperature evolution of the $q_{\text{ortho-II}}$ satellite profiles along k (panel a) and h (panel b). The bright and dark color corresponds respectively to the higher and lower intensities of the diffraction spots. The temperature evolution of width of the $q_{\text{ortho-II}}$ satellite reflections along b^* (panel c) and a^* direction (panel d) is plotted. Normalized intensity of the $q_{\text{ortho-II}}$ superlattice peak as a function of temperature is shown in panel (e). Circles (blue online) and squares (red online) represent the data collected during the cooling and heating thermal cycles, respectively. Panel (f) : variation in the average number of oxygen chains in each ortho II puddle in the horizontal (triangles) and vertical (squares) direction as a function of temperature in the warming followed by the cooling process. The difference between the size of the horizontal and vertical ortho-II puddles (large black dots) in the temperature range $340\text{K} < T < 380\text{K}$ during the warming process provides evidence for spontaneous symmetry breaking in the fluctuation regime at the phase transition.

The width of the diffraction profiles in h -direction in panel (d) probes the disorder in Ortho-II puddles transverse to the chains direction i.e. provides the number of chain fragments in a puddle. We see above the transition temperature at 350K in agreement with previous works [25,26] and the presence of fluctuations with very small nanoscale puddles up to 400K. In this fluctuation regime of bubbles in the range 350-380K we observe a spontaneous symmetry breaking shown in panel (f). The cuts of the streaks in the h -direction transverse to the chain direction becomes broader as expected for the horizontal puddles while it becomes narrower for the vertical

puddles. This process of symmetry breaking has been already used for growing samples with collinear Ortho-II puddles forming untwined orthorhombic crystals.

The cooling ramp with the same rate was made down to 200 K. The hysteresis shown in Fig. 4 demonstrates that once the nano-scale puddles, of Ortho-II oxygen chains, are formed, they cannot be reformed on the average in a reversible way with the same size in the time scale of the experiment.

Discussion. We have investigated the variation of the ortho-II puddles size from point to point with micro-meter resolution using a novel mixed k-space and r-space probe of bulk heterogeneity combining high wave number resolution with micrometer-scale spatial resolution.

The scanning μ XRD is similar to transmission electron microscopy (TEM), but without the complication of electron beam damage. In fact the electron beam heating of the thin crystals can change the mobile oxygen content y and generate transient non-equilibrium surface structures that mask intrinsic bulk effects. Therefore information of finite size ordering properties as well as temperature dependent properties is not achievable by TEM.

The application of scanning μ XRD for imaging the nanoscale puddles with Ortho-II phase show the presence of a nematic phase of nano-scale Ortho-II puddles in a sample very close to the superconductor-insulator phase transition. The network of the Ortho-II puddles is made of different puddles ranging between 3 and 12 oxygen chains. The scanning μ -XRD and the temperature treatments show that the local structure in YBCO deviates from the ideal one. The crystal shows nanoscale puddles with Ortho-II superstructure. We have seen a relevant structure dependence with temperature in agreement with previous high resolution XRD data, where temperature treatments modify the density and elongation of the Cu-O chains [42]. The formation of nanoscale ordered grains in YBCO with Ortho-II lattice in the basal plane is highly relevant for the electronics of the system and for models of superconductor-to-insulator transition [19,20]. The oxygen chain puddles have the Ortho-II lattice superstructure, like the $\text{YBa}_2\text{Cu}_3\text{O}_{6.5}$ which shows band folding and Fermi surface reconstruction measured by photoemission and quantum oscillations experiments [47,48]. The nanoscopic phase separation of the oxygen puddles shown here, using μ XRD could explain why zero and transverse field μ SR experiments have shown the coexistence of antiferromagnetic short range magnetism with superconductivity in YBCO with $6.37 < y < 6.39$ [49]. In fact, since the average oxygen concentration is 6.33 and the local oxygen concentration in the oxygen ordered puddles is 6.5 in the intercalated spatial portions the oxygen concentration y has to be smaller than 6.33. The oxygen puddles are expected to cover 66% of the space and therefore they percolate while the nanoscopic magnetic portions do not percolate, that explains why neutron scattering experiments do not find a static antiferromagnetism [49]. On the other hand, both neutron scattering and μ SR experiments agree with the presence of two energy scales and short-ranged correlations. A similar

granular disorder has been found in single crystals of $\text{La}_2\text{CuO}_{4+y}$ [11,22,38] and of $\text{Bi}_2\text{Sr}_2\text{CaCu}_2\text{O}_{8+y}$ [25] using scanning μ XRD.

Our non-invasive technique μ XRD probes portions of the single crystals of one micron size, much smaller than those seen by neutron diffraction and previous X-ray diffraction [26] and therefore allows us to measure the formation of nanocrystalline puddles with spatial resolution.

Conclusion We have used scanning μ XRD to probe the microscopic spatial inhomogeneity in $\text{YBa}_2\text{Cu}_3\text{O}_{6.33}$, which is cannot be visualized through standard averaged X-ray diffraction. The granular nanoscopic phase separation has been visualized with one micron resolution showing the network of the Ortho-II oxygen ordered puddles. The probability distribution of the puddles of oxygen chains has been obtained by μ XRD. This work shows that the size of the nanoscale oxygen ordered puddles in Y123 near the superconductor-insulator phase transition is much smaller than in $\text{La}_2\text{CuO}_{4+y}$ with a larger misfit strain.

Acknowledgments: We thank Ruixing Liang, D.-A. Bonn, and Walter-N. Hardy of the Department of Physics of the University of British Columbia, for proving us with the crystals and for helpful discussions.

References

- [1] A. Bianconi, Solid State Communications **89**, 933 (1994)
- [2] M. K. Wu, J. R. Ashburn, C. J. Torng, P. H. Hor, R. L. Meng, L. Gao, Z. J. Huang, Y. Q. Wang, and C. W. Chu, *Phys. Rev. Lett.* **58**, 908 (1987).
- [3] J. Zaanen and O. Gunnarsson, Physical Review B **40**, 7391 (1989)
- [4] A. Bianconi, A. Congiu-Castellano, M. De-Santis, P. Rudolf, P. Lagarde, A. M. Flank, and A. Marcelli, Solid State Communications **63**, 1009 (1987)
- [5] T. Egami and S. J. L. Billinge, Underneath the Bragg Peaks, Volume 16: Structural Analysis of Complex Materials (Pergamon Materials Series) (Pergamon, 2003).
- [6] A. Bianconi, N. L. Saini, A. Lanzara, M. Missori, T. Rossetti, H. Oyanagi, H. Yamaguchi, K. Oka, and T. Ito, Physical Review Letters **76**, 3412 (1996).
- [7] A. Bianconi, N.L Saini, S. Agrestini, D. Di Castro, G. Bianconi International Journal of Modern Physics B **14**, 3342 (2000) ; A. Bianconi, D. Di Castro, G. Bianconi et al. Physica **C 341**, 1719 (2000)
- [8] A. Bianconi, S. Agrestini, G. Bianconi, D. Di Castro, and N. L. Saini, Journal of Alloys and Compounds **317-318**, 537 (2001)
- [9] P. Littlewood, *Nat Mater* **10**, 726 (2011).
- [10] T. H. Geballe, & M. Marezio *Physica C: Superconductivity*, **469**, 680 (2009).
- [11] N. Poccia, A. Ricci, G. Campi, M. Fratini, A. Puri, D. D. D. Gioacchino, A. Marcelli, M. Reynolds, M. Burghammer, N. L. L. Saini, et al. , *Proc. Nat. Acad. Sci. USA* **109**, 15685 (2012).
- [12] L. P. Gor'kov & G. B. Teitel'baum *Phys. Rev. B*, **82**, 020510 (2010).
- [13] K. I. Kugel, A. L. Rakhmanov, A. O. Sboychakov, N. Poccia, and A. Bianconi *Phys. Rev. B*, **78**, 165124 (2008)
- [14] D. Innocenti, A. Ricci, N. Poccia, G. Campi, M. Fratini, and A. Bianconi, J. of Superconductivity and Novel Magn. **22**, 529 (2009)
- [15] A. Bianconi and M. Missori, Solid State Communications **91**, 287 (1994).
- [16] A. Perali, A. Bianconi, A. Lanzara, and N. L. Saini, Solid State Communications **100**, 181 (1996)
- [17] V Kresin, Y Ovchinnikov, & S Wolf *Physics Reports*, **431**, 231 (2006)
- [18] E. V. L. de Mello *EPL (Europhysics Lett.)* **98**, 57008 (2012)
- [19] G. Bianconi *Phys. Rev. E*, **85**, 061113 (2012).
- [20] G. Bianconi *Journal of Statistical Mechanics: Theory and*

Experiment [2012, P07021 \(2012\)](#).

- [21] J. Zaanen *Nature* [466, 825 \(2010\)](#)
- [22] M. Fratini, N. Poccia, A. Ricci, G. Campi, M. Burghammer, G. Aeppli, and A. Bianconi, *Nature* [466, 841 \(2010\)](#).
- [23] N. L. Saini, H. Oyanagi, T. Ito, V. Scagnoli, M. Filippi, S. Agrestini, G. Campi, K. Oka, and A. Bianconi, *The European Physical Journal B - Condensed Matter and Complex Systems* [36, 75 \(2003\)](#)
- [24] E. S. Božin, G. H. Kwei, H. Takagi, & S. J. L. Billinge *Physical Review Letters*, [84, 5856 \(2000\)](#).
- [25] N. Poccia, G. Campi, M. Fratini, A. Ricci, N. L. Saini, and A. Bianconi *Phys. Rev. B* [84, 100504 \(2011\)](#)
- [26] G. Campi, E. Cappelluti, T. Proffen, X. Qiu, E. S. Bozin, Billinge, S. Agrestini, N. L. Saini, and A. Bianconi, *The European Physical Journal B - Condensed Matter and Complex Systems* [52, 15 \(2006\)](#).
- [27] V. Ksenofontov, G. Wortmann, S.A. Medvedev, V. Tsurkan, J. Deisenhofer, A. Loidl, and C. Felser, *Phys. Rev. B* [84, 180508 \(2011\)](#)
- [28] A. Charnukha, J. Deisenhofer, D. Pröpper, M. Schmidt, Z. Wang, Y. Goncharov, A. N. Yaresko, V. Tsurkan, B. Keimer, A. Loidl, et al. , *Phys. Rev. B* [85, 100504 \(2012\)](#).
- [29] A. Ricci, N. Poccia, G. Campi, B. Joseph, G. Arrighetti, L. Barba, M. Reynolds, M. Burghammer, H. Takeya, Y. Mizuguchi, et al. , *Phys. Rev. B* [84, 060511 \(2011\)](#)
- [30] E. Dagotto *Nanoscale phase separation and colossal magnetoresistance : the physics of manganites and related compounds*. Springer (2003).
- [31] J. D. Jorgensen, S. Pei, P. Lightfoot, H. Shi, A. P. Paulikas, and B. W. Veal, *Physica C: Superconductivity* [167, 571 \(1990\)](#)
- [32] B. W. Veal, A. P. Paulikas, H. You, H. Shi, Y. Fang, and J. W. Downey, *Phys. Rev. B* [42, 6305 \(1990\)](#).
- [33] G. Ceder, R. McCormack, and D. de Fontaine, *Physical Review B* [44, 2377 \(1991\)](#)
- [34] H. Friis Poulsen, N. Hessel Andersen, J. Vrtting Andersen, H. Bohrt, and O. G. Mouritsen, *Nature* [349, 594 \(1991\)](#).
- [35] G. Yu, C. H. Lee, A. J. Heeger, N. Herron, E. M. McCarron, L. Cong, G. C. Spalding, C. A. Nordman, and A. M. Goldman, *Phys. Rev. B* [45, 4964 \(1992\)](#).
- [36] S. Sanna, G. Allodi, G. Concas, A. D. Hillier, and R. De Renzi, *Phys. Rev. Lett.* [93, 207001 \(2004\)](#)
- [37] C. L. Johnson, J. K. Bording, and Y. Zhu, *Phys. Rev. B* [78, 014517 \(2008\)](#)
- [38] N. Poccia, M. Fratini, A. Ricci, G. Campi, L. Barba, A. Vittorini-Orgeas, G. Bianconi, G. Aeppli, and A. Bianconi, *Nature Materials* [10, 733 \(2011\)](#).
- [39] R. Liang, D. A. Bonn, and W. N. Hardy, *Physica C*, [336, 57 \(2000\)](#)
- [40] R. Liang et al., *Physica C*, [383, 1 \(2002\)](#).
- [41] J. Stempfer, I. Zegkinoglou, U. Rütt, Zimmermann, C. Bernhard, C. T. Lin, Th, and B. Keimer, *Physical Review Letters* [93, 157007 \(2004\)](#)
- [42] M. von Zimmermann, J. R. Schneider, T. Frello, N. H. Andersen, J. Madsen, M. Käll, H. F. Poulsen, R. Liang, P. Dosanjh, W. N. Hardy, *Phys. Rev. B* [68, 104515 \(2003\)](#)
- [43] Ruixing Liang, D.A. Bonn, W.N. Hardy *Phil. Mag.* [92, 2356 \(2012\)](#).
- [44] Ruixing Liang, D.A. Bonn, W.N. Hardy, *Physica C*. [304, 105 \(1998\)](#).
- [45] Ruixing Liang, D.A. Bonn, W.N. Hardy, J.C. Wynn, K.A. Moler, L. Lu, S. Larochele, L. Zhou, M. Greven, L. Lurio, S.G.J. Mochrie *Physica C* [383, 1 \(2002\)](#).
- [46] J. Garcia, A. Bianconi, M. Benfatto, and C. R. Natoli, *Le Journal de Physique Colloques* [47, C8 \(1986\)](#)
- [47] Y. Sassa, M. Radović, M. Maansson, E. Razzoli, X. Y. Cui, S. Pailhès, S. Guerrero, M. Shi, P. R. Willmott, F. M. Granozio, et al., *Phys. Rev. B* [83, 140511 \(2011\)](#)
- [48] D. Fournier, G. Levy, Y. Pennec, J. L. McChesney, A. Bostwick, E. Rotenberg, R. Liang, W. N. Hardy, D. A. Bonn, I. S. Elfimov, et al., *Nature Physics* [6, 905 \(2010\)](#)
- [49] C. Stock, W. J. L. Buyers, Z. Yamani, C. L. Broholm, J. H. Chung, Z. Tun, R. Liang, D. Bonn, W. N. Hardy, and R. J. Birgeneau, *Phys. Rev. B* [73, 100504 \(2006\)](#).